Bioorganic & Medicinal Chemistry 18 (2010) 366–376

Contents lists available at ScienceDirect

Bioorganic & Medicinal Chemistry

journal homepage: www.elsevier.com/locate/bmc

Detection of multiple network-based allosteric interactions between peptides and arrays of DNA binding sites

Karen K. L. Kao [a], Jonathan C. T. Huang [a], Chi-Kai Yang [a], Kee-Ching G. Jeng [b], Jung-Cheng Chang [a], Wen-Chen Yao [a], S. C. Hsien [a], Michael J. Waring [c], Ming-Hua Chen [d], Lin Ma [d], Leung Sheh [a,*]

[a] Department of Chemistry and Life Science Center, Tunghai Christian University, Taichung 407, Taiwan, ROC
[b] Department of Medical Research, Taichung Veterans General Hospital, Taichung 405, Taiwan, ROC
[c] Department of Pharmacology, University of Cambridge, Tennis Court Road, Cambridge CB2 1PD, England, United Kingdom
[d] Shaw College, The Chinese University of Hong Kong, Shatin, N.T., Hong Kong

ARTICLE INFO

Article history:
Received 17 September 2009
Revised 22 October 2009
Accepted 24 October 2009
Available online 31 October 2009

Keywords:
DNA cooperative networks
Footprinting
Circular dichroism
Molecular recognition
Peptides

ABSTRACT

Quantitative DNase I footprinting shows that three designed peptides containing *N*-methylpyrrole (Py) moieties display different types of network-based allosteric communication in binding to DNA: circuit type, incomplete-circuit type, and non-circuit type characterized by interstrand bidentate interactions. Positive cooperative binding of all three peptides to individual DNA binding sites is commonly observed. CD spectral characterization of the interaction between peptides and model undecanucleotide duplexes is consistent with the footprinting results and supports the allosteric model. This study provides insights relating to the interaction network nature of allostery in complex DNA–small molecule interactions.

1. Introduction

Current studies on sequence-selective binding of small ligands to DNA play an essential part in the advance towards understanding molecular aspects of the modulation of gene expression. This work is also important for the advancement of structural biochemistry research and drug design.[1–4] Extensive studies have been carried out with small ligands that are capable of sequence-specific recognition of DNA including drugs,[1–3] antitumor antibiotics,[4–7] netropsin/distamycin and its analogues,[8–13] and synthetic peptides.[14–17]

Previously we introduced a novel XPRK peptide motif as a basis for sequence-selective interaction studies.[14–17] The design of this motif stems from a naturally occurring SPXX motif[18,19] found in repeating sequences in histones, steroid hormone receptors, various segmentation gene products and some oncogene products. It was suggested that the SPXX motif assumes a β-turn stabilized by two hydrogen bonds, and that the side chains of the two basic residues engage in salt bridges with the DNA phosphate groups.[18,19] Further conjugation of two XPRK motifs with a tract of 4-amino-1-methylpyrrole-2-carboxylic acid residues (Py) afforded peptides with higher affinity toward DNA sequences incorporating three or four consecutive W (A or T) base pairs.

Extensive research spanning nearly fifty years has been devoted to the allosteric behavior of macromolecules such as proteins[21] because allostery is recognized as a central process in biological control governing biochemical efficiency and energy metabolism. By contrast, studies on allosteric aspects of DNA–ligand interactions have been much less popular than protein–ligand interactions. This prompted us to focus on molecular aspects of cooperative interactions between peptides and DNA. In our early sequence-specificity studies with synthetic molecules containing both the XPRK motif[14–17] as well as the polyamide motif we found a number of peptides that exhibit notable sequence-selectivity in binding to particular sites on the DNA duplex. Among these peptides we identified a nonapeptide His-Hyp-Arg-Lys-$(Py)_3$-Lys-Arg-NH_2 (PyHyp-9) and a dodecapeptide His-Hyp-Arg-Lys-$(Py)_4$-His-Hyp-Arg-Lys-NH_2 (PyHyp-12) that displayed significant cooperativity in binding to DNA. We also established that quantitative footprinting is the method of choice for investigating allosteric interactions between multiple binding sites on complementary DNA strands since it is difficult for most spectroscopic techniques to characterize multiple binding sites.

It is generally recognized that network-based interactions between multiple elements play a part in many biochemical and physiological processes in nature. Recently we proposed a net-

* Corresponding author. Tel.: +886 4 23590248; fax: +886 4 23590426.
E-mail address: Lsheh@thu.edu.tw (L. Sheh).

0968-0896/$ - see front matter © 2009 Elsevier Ltd. All rights reserved.
doi:10.1016/j.bmc.2009.10.048

work-based DNA–peptide allosteric model[17,20] that features intercommunicating binding sites in fragments of the latent membrane protein-1 gene from a pathogenic Epstein–Barr virus variant derived from nasopharyngeal carcinoma. In the present study we further explore whether such network-based allosteric behavior can be detected in common DNA motifs containing consecutive A's and T's. To this end we compare the physicochemical binding parameters of the newly designed peptides PyHyp-9 and PyHyp-12 with that of the parent peptide His-Pro-Arg-Lys-$(Py)_4$-His-Pro-Arg-Lys-NH_2 (PyPro-12) using quantitative DNase I footprinting. Cooperativity is assessed using the Hill equation which is well established for that purpose.[17,23–25] To furnish insights into possible mechanisms based on DNA conformational changes circular dichroism spectroscopic results are also reported.

2. Results and discussion

Since the initial objective of this study was to investigate the molecular basis underlying cooperativity between multiple peptide recognition sites, a complementary pair of 5′-^{32}P-labeled pBR322 fragments[15] comprising a 158-mer duplex (upper strand 5′-^{32}P-labeled) and a 135-mer duplex (lower strand 5′-^{32}P-labeled) were employed as substrates. Previous footprinting studies showed that the XPRK series of peptides bind preferentially to four sites on the upper and lower strands where the complementary sequences d(AAAA)–d(TTTT) and d(AAA)–d(TTT) occur around positions 108–111 and 83–85, respectively. The design of the new peptides PyHyp-9 and PyHyp-12 stems from the parent peptide PyPro-12 (previously named PyH-12).[15] In peptides PyHyp-9 and PyHyp-12 proline is replaced by hydroxyproline, furnishing extra hydroxyl groups for additional hydrogen bonding. The nonapeptide PyHyp-9 represents a new design in which the number of Py residues is reduced to three and the *C*-terminal tetrapeptide portion (-His-Hyp-Lys-Arg-NH_2 in peptide PyHyp-12) is truncated to a dipeptide (-Lys-Arg-NH_2).

Peptide PyHyp-9 displays a strong sequence preference for consecutive arrays of A's and T's in DNA (Fig. 1). At present the nonapeptide PyHyp-9 is the smallest peptide containing enough amino acid residues to evince satisfactory footprints in the XPRK series. Quantitative footprinting by this and other peptides (Figs. 1–3, 4A–C) on the complementary strands provides valuable information about possible interstrand bidentate interactions[15,22] as well as intrastrand H-bond interactions[22] involving the side chains and amino protons of the peptides bonding to bases in the complementary DNA strands. These specific H-bond interactions between the peptides and DNA bases are well-recognized mediators of sequence recognition by ligands including proteins as well as small molecules[15,22] Interstrand bidentate interactions can be assigned from the differential cleavage plots at nucleotide positions where significant coincident DNase I blockages are observed (Fig. 4A–C).

On the upper strand, peptide PyHyp-9 binds strongly to two sites (Figs. 1 and 4A): position U107–113, corresponding to the sequence 5′-GAAAATA-3′ which shows marked positive cooperativity (n_H = 2.2); and position U84–89 comprising the sequence 5′-AA-TACC-3′, also associated with positive cooperativity (n_H = 2.2). On the complementary lower strand, PyHyp-9 footprints at two sites:

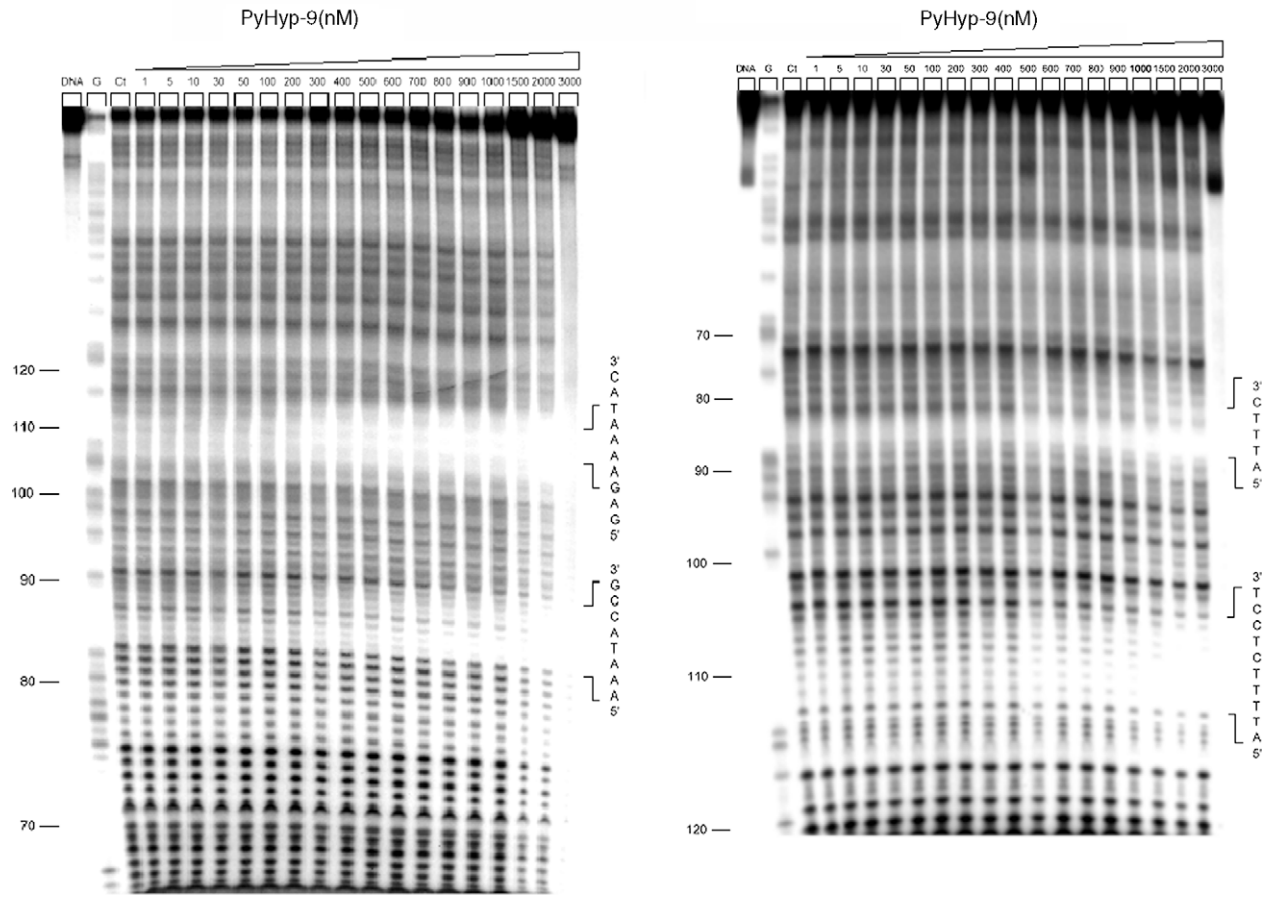

Figure 1. Autoradiograph showing DNase I footprinting of peptide PyHyp-9 on DNA duplexes labeled with [γ-^{32}P]ATP on the 5′ end: 5′-^{32}P-labeled 158-mer upper strand, left panel; and 5′-^{32}P-labeled 135-mer lower strand, right panel. PyHyp-9 was equilibrated with the DNA in 5 mM sodium cacodylate buffer, pH 6.5 at 37 °C for 60 min before nucleolytic cleavage. G represents a Maxam–Gilbert guanine sequencing track and Ct shows a DNase I digestion control lane.

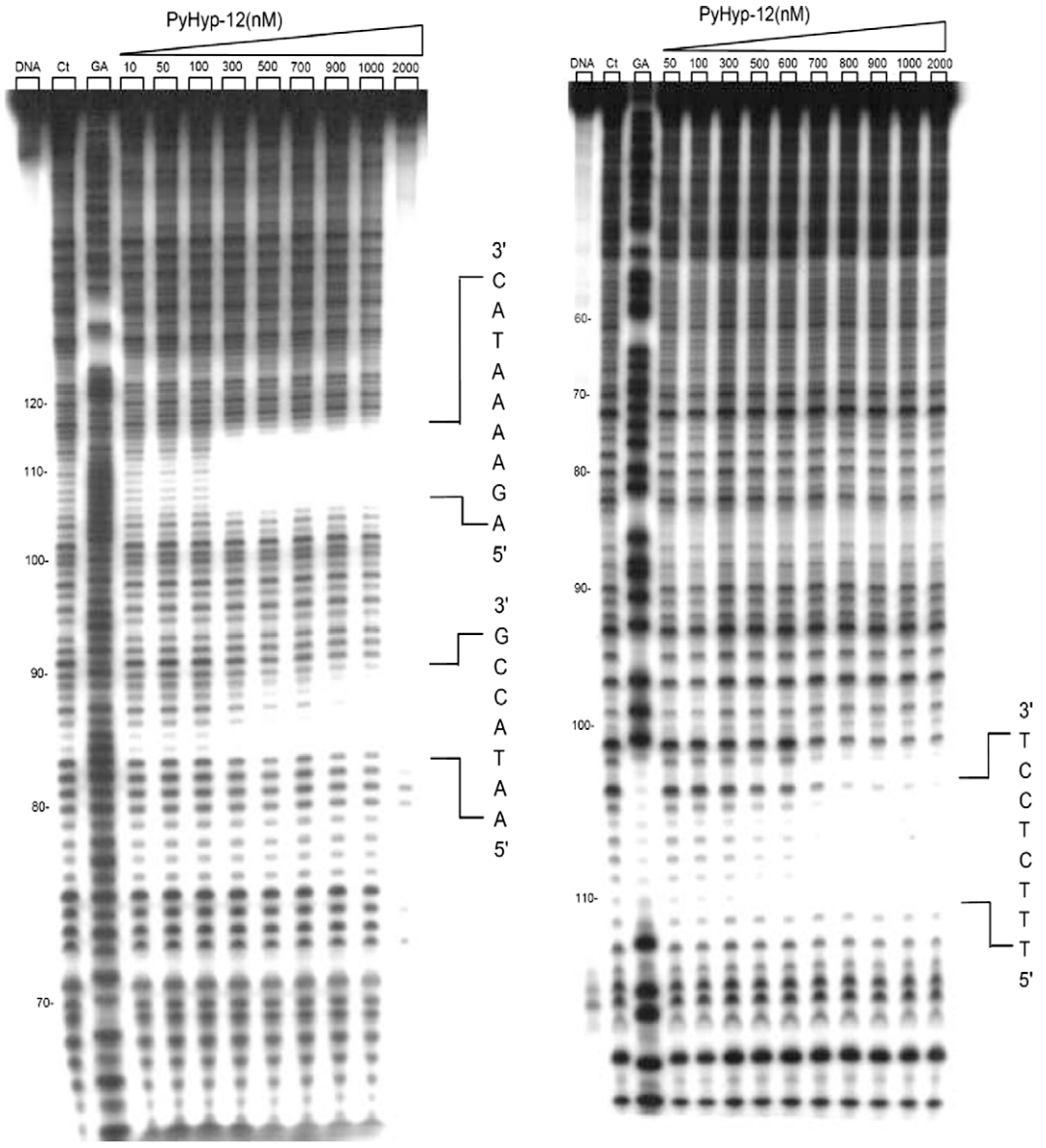

Figure 2. DNase I footprinting of peptide PyHyp-12 on DNA duplexes labeled with [γ-^{32}P]ATP on the 5′ end: 5′-^{32}P-labeled 158-mer upper strand, left panel; and 5′-^{32}P-labeled 135-mer lower strand, right panel. Reaction conditions as in the legend to Figure 1.

position L111–103, corresponding to the sequence 5′-TTTTCTCCT-3′ (n_H = 2.0), and position L84–83, comprising the sequence 5′-TT-3′ (n_H also 2.0). Examination of the differential plot thus allows us to assign interstrand bidentate interactions around positions 84 and 107–111. It is noteworthy that the nonapeptide displays significant positive cooperativity at all four binding sites on both strands.

The DNase I footprinting profile of peptide PyHyp-12 (Figs. 2 and 4B) appears to be quite different from that of the parent peptide PyPro-12. On the upper strand, peptide PyHyp-12 produces a broad DNase I blockage site around position U106–114 corresponding to the sequence 5′-AGAAAATAC-3′, displaying weak positive cooperativity (n_H = 1.4). Another blockage site occurs at position U84–88, comprising the sequence 5-AATAC-3′ displaying similarly weak positive cooperativity (n_H = 1.5). On the lower strand, PyHyp-12 binds preferentially to a broad site around position L110–103, corresponding to the sequence 5′-TTTCTCCT-3′ showing the same weak positive cooperativity (n_H = 1.4), but the binding site around position L84–83 that appears with peptide PyHy-9 is completely missing. In this case the differential cleavage plots indicate that for PyHyp-12 interstrand bidentate interactions can only be assigned around position 106–110. It is envisaged that these interstrand hydrogen bond interactions are involved in relaying conformational changes between local DNA sites, thereby facilitating binding of further peptide molecules across the complementary strands.

We repeated footprinting experiments on the parent peptide PyPro-12[15] using a wider concentration range (Figs. 3 and 4C). On the upper strand PyPro-12 binds quite well around position U84–90, comprising the sequence 5′-AATACCG-3′, showing some negative cooperativity (n_H = 0.7). Another broad blockage site occurs around position U106–116, comprising the sequence 5′-AGAAAATACCG-3′, showing weak positive cooperativity (n_H = 1.2). On the lower strand, corresponding blockage sites also appear around positions L85–83 (n_H = 1.1) and L110–105 (n_H = 1.5) that indicate binding of peptide molecules to sites on the opposite complementary strand, also manifesting modest positive cooperativity (Fig. 4C). So for this peptide interstrand bidentate interactions[15,22] can be assigned around position 84–85 as well as 106–110. The

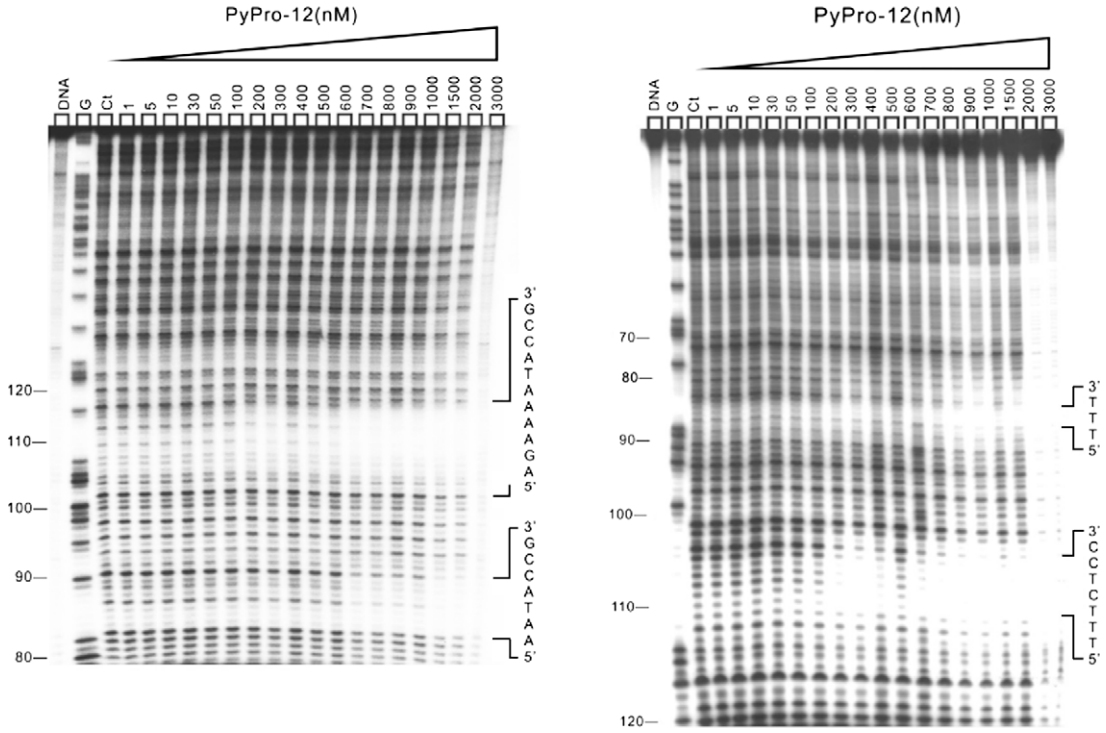

Figure 3. DNase I footprinting of peptide PyPro-12 on DNA duplexes labeled with [γ-^{32}P]ATP on the 5′ end: 5′-^{32}P-labeled 158-mer upper strand, left panel; and 5′-^{32}P-labeled 135-mer lower strand, right panel. Reaction conditions as in Figure 1.

apparent binding constant K_a of the three peptides on the four major binding sites of the pBR322 fragments lie rather even in the range of 2.2–3.8 $\times$ 10^6 M^{-1}, with the exception that peptide PyPro-12 has a rather high K_a (6.7 $\times$ 10^7 M^{-1} on position U80–84) (Table 1). Similarly, the apparent binding constant of peptides PyHyp-12 and PyHyp-9 on binding to the S-81 DNA also lie rather steady in the range of 1.4–2.5 $\times$ 10^6 M^{-1} (Table 2).

In view of the broad DNase I blockage sites seen with all three peptides, we envisage that two peptide molecules may be capable of binding in a dimeric head-to-head or head-to-tail fashion to some or all of these binding sites (Fig. 5). Several modes of binding of peptide molecules to complementary or adjacent binding sites are possible that might lead to cooperative binding. Interaction of a peptide molecule in a sequential manner with one sub-site (inside a binding site) on one DNA strand could facilitate the binding of a molecule to the other sub-site on the same strand. On the other hand, binding of a peptide molecule to one site might induce local DNA conformational change(s) mediated by interstrand bidentate interactions and facilitate sequential or concerted binding of further peptide molecules to an opposite site on the complementary strand. Of course, binding of peptide molecules to one site could invoke conformational change(s) and facilitate or hinder peptide binding to a neighboring site on the same strand. Thus, cooperative (or anti-cooperative) binding distributed between an array of binding sites may establish a network of cooperativity interconnecting several allosteric sites (Fig. 5).

To assess the nature and magnitude of allosteric communication between the d(AAAA)–d(TTTT) and d(AAA)–d(TTT) binding loci in the pBR322 fragments we designed a new 81-mer duplex (S-81) containing a single d(AAAA)–d(TTTT) sequence. The apparent size (number of nucleotides) of each binding locus was found to vary for individual peptides (Table 2). Quantitative footprinting experiments were carried out for peptides PyHyp-12 and PyHyp-9 binding to the 5′-^{32}P-labeled upper and lower strand duplexes (Supplementary data). Strikingly, the n_H values for peptides PyHyp-12 and PyHyp-9 binding to the 81-mer duplexes containing a single binding locus (Table 2) are significantly higher than those of the 158-mer and 135-mer duplexes containing both binding loci (Table 1). This suggests the existence of some negative cooperative effect associated with binding to the d(AAA)–d(TTT) and d(AAAA)–d(TTTT) positions, lowering the positive cooperativity between adjacent and complementary sub-sites, and resulting in smaller observed values of n_H at both sites, mediated over an intervening sequence of 12–14 base pairs.

Based on the quantitative footprinting behavior of the three peptides, summarized in Table 1, we have proposed network-based models in an effort to interpret the complex communication between DNA–peptide allosteric binding sites (Fig. 5). The 158-mer and 135-mer fragments used here contain two peptide binding loci: around position 83–89, comprising the d(AAA)–d(TTT) sequence, and position 103–116 comprising the d(AAAA)–d(TTTT) sequence. Each locus seems to afford two complementary sites that consist of two to four sub-sites, depending on individual peptides. In the model, conformational changes induced at one position affect binding to a neighboring site, and interstrand bidentate interactions are envisaged as playing an important role in relaying conformational changes between sites on the complementary strands, facilitating the binding of further peptide molecules. The different models for PyHyp-9, PyHyp-12 and PyPro-12 primarily reflect differences in the relay of conformational change between opposite sites on complementary strands via interstrand bidentate interactions. It is apparent that peptides PyHyp-9 and PyPro-12 form a circuit type of a communication: the allosteric communication between binding sites is complete. On the other hand, the communication in the DNA binding of peptide PyHyp-12 appears to be discontinuous and is referred to as an incomplete-circuit type. Footprinting experiments on the 81-mer duplex (S-81) containing a single d(AAAA)–d(TTTT) sequence (Table 2) suggest that the allosteric relay of peptide binding to adjacent sites between the d(AAA)–d(TTT) and d(AAAA)–d(TTTT) positions spanning over

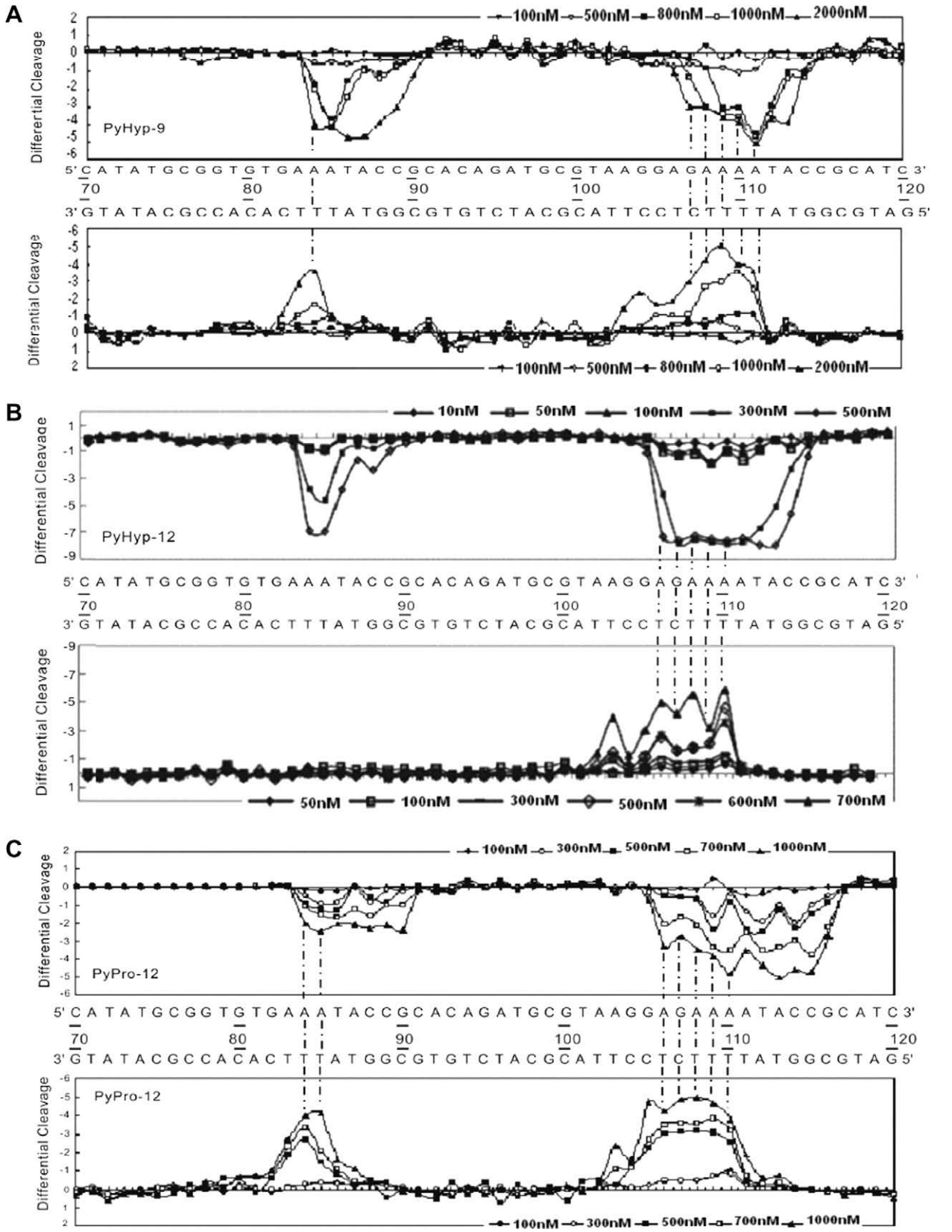

Figure 4. Differential cleavage plots comparing the susceptibility of DNA fragments to DNase I cleavage after incubation with each peptide in cacodylate buffer at room temperature for 60 min. In each panel A, B, C the upper traces represent the differential cleavage plot for a given peptide bound to the 5′-^{32}P-labeled upper strand (158-mer) DNA fragment; the lower traces represent the corresponding plots for each peptide bound to the 5′-^{32}P-labeled lower strand (135-mer) DNA fragment. The vertical dotted lines between DNA bases represent assignment of interstrand bidentate interactions where significant coincident H-bonding interactions occur between complementary bases in both strands.

Table 1
Physicochemical parameters for binding of peptides to recognition sites in pBR322 fragments: complementary 5′-^{32}P-labeled upper strand (158-mer) and lower strand (135-mer) DNA duplexes at 37 °C

Peptide	Binding site position	Recognition sequence	K_a (M^{-1})	n_H	Interstrand bidentate interactions (position)
PyHyp-9	U84–89	5′-AATACC-3′	2.5×10^6	2.2	84
	U107–113	5′-GAAAATA-3′	3.8×10^6	2.2	107–111
	L84–83	5′-TT-3′	2.7×10^6	2.0	
	L111–103	5′-TTTTCTCCT-3′	2.2×10^6	2.0	
PyHyp-12	U84–88	5′-AATAC-3′	2.5×10^6	1.5	106–110
	U106–114	5′-AGAAAATAC-3′	3.4×10^6	1.4	
	L110–103	5′-TTTCTCCT-3′	3.4×10^6	1.4	
PyPro-12	U80–94	5′-AATACCG-3′	6.7×10^7	0.7	84–85
	U106–116	5′-AGAAAATACCG-3′	3.2×10^6	1.2	106–110
	L85–83	5′-TTT-3′	3.7×10^6	1.1	
	L110–105	5′-TTTCTCC-3′	3.8×10^6	1.5	

K_a and n_H are the apparent association constant and Hill coefficient determined from concentration-dependent DNase I footprinting studies, respectively. The binding site positions on the upper and lower strands are abbreviated as U and L, respectively. Interstrand bidentate interactions are assigned where there are coincident effects on complementary bases in both strands.

Table 2
Physicochemical parameters for binding of peptides to the S-81 DNA: complementary 5′-^{32}P-labeled upper strand (81-mer) and lower strand (81-mer) duplexes at 37 °C

Peptide	Binding site position	Recognition sequence	K_a	n_H	Interstrand bidentate interactions (position)
PyHyp-9	U44–48	5′-AAAAT-3′	2.1×10^6	3.9	44–47
	L47–41	5′-TTTTCTC-3′	1.9×10^6	3.2	
PyHyp-12	U44–48	5′-AAAAT-3′	1.4×10^6	2.3	44–46
	L46–42	5′-TTTCT-3′	2.5×10^6	2.6	

Details as in the legend to Table 1.

an intervening sequence of 12–14 base pairs is affected by some negative cooperative effect (Fig. 5).

Seeking further evidence for conformational changes accompanying the molecular recognition process we resorted to circular dichroism spectroscopy (CD) as a means of probing changes in the helical structure associated with peptide–DNA binding. Two 11-mer deoxyribonucleotide duplexes were synthesized, d(GGAGA AAATAC)–d(GTATTTTCTCC) (4A–4T) and d(GTGAAATACCG)–d(CG GTATTTCAC) (3A–3T), corresponding to the recognition sites of the pBR322 fragments at positions 104–114 and 80–90 separately. With both duplexes a negative CD band around 253 nm and a positive band around 274 nm were observed (Fig. 6A). On increasing the concentration of peptide PyHyp-9 added to duplex 4A–4T, the 274 nm band is red-shifted to about 278 nm and a near-isoelliptic point appears suggesting a predominantly two-component binding process (Fig. 6B). This positive CD band extends as a shallow broad dose-dependent positive enhancement to 350 nm. In the difference spectrum (Fig. 6C) it can be seen that binding of peptide PyHyp-9 to the duplex results in dose-dependent CD intensity enhancement of two neighboring negative bands centering around 243 nm and 268 nm. Another curious feature of Figure 6C is a blue-shifted positive CD band around 273 nm induced by PyHyp-9 at low concentration (0.2 μM).

Addition of PyHyp-9 to the DNA duplex 3A–3T also induces a red-shift of the positive band at 274 nm to 281 nm with quite a good isoelliptic point at 283 nm (Fig. 6D). Again this positive band extends as a shallow broad band to about 350 nm. In the difference spectra two negative bands around 248 nm and 267 nm are observed (Fig. 6E), and at low concentrations of PyHyp-9 (0.2 μM and 1.0 μM), the induced positive CD band appears blue-shifted to about 282 nm. Odd spectral changes observed at low peptide concentrations are not entirely unexpected given the anomalous situation that might prevail when small numbers of ligand molecules are bound, probably largely to isolated sites, before propagated effects mediated via early conformational changes become predominant.

By contrast, titration of peptide PyHyp-12 versus the 4A–4T duplex produces a dose-dependent negative CD enhancement band around 250 nm as well as two strong positive CD enhancement bands around 283 nm and 325 nm (Fig. 7A). In the difference spectra two negative bands are seen around 243 nm and 268 nm as well as positive bands around 288 nm and 322 nm (Fig. 7B). A fairly consistent isoelliptic point also occurs near 280 nm, suggesting mainly a two-component binding process. Titration of PyHyp-12 versus the 3A–3T duplex (Fig. 7C) induces similar CD spectral changes to those observed with the 4A–4T duplex. In the difference spectra, there are strong and minor negative bands around 266 and 249 nm, while two strong positive CD bands appear around 282 and 325 nm (Fig. 7D).

For peptide PyHyp-9, the distinct separation of two unusual neighboring negative CD bands around 243 nm and 268 nm as well as the strong red-shifted positive bands indicate that significant local conformational changes are indeed induced in the duplex by the binding of the peptide, most likely resulting in the positively cooperative binding observed. Moreover, in the difference spectra (Figs. 6C and E), it is apparent that the enhancement of the CD bands is correlated with peptide–DNA binding stoichiometry. Accordingly we propose a three-step binding process (Fig. 8). At [peptide]/[duplex] ratios of 0.5–2, one molecule of PyHyp-9 or PyHyp-12 binds to the d(AAAA)–d(TTTT) or d(AAA)–d(TTT) locus, most probably in the minor groove. However, at [peptide]/[duplex] ratios above 1 and up to about 4, there is often a steeper variation in ellipticity consistent with strong positive cooperativity arising from binding of the first molecule facilitating the binding of a second molecule to form a 2:1 complex. At [peptide]/[duplex] ratios above 4.0, the progressive but smaller increase in $\Delta\theta$ suggests that more peptide molecules begin to bind non-selectively, perhaps occupying the wide major groove which can accommodate more peptide molecules than the minor groove. This idea is consistent with the footprinting studies which clearly indicate that peptide concentrations above 2 μM can result in non-sequence selective binding to DNA (Figs. 1 and 2).

There are signs that the peptides may bind in dimeric head-to-head or head-to-tail fashion to the d(AAAA)–d(TTTT)-containing 11-mer duplex with positive cooperativity. For peptide PyHyp-12, in addition to a positive CD band around 280 nm the appearance of a stronger positive band centered around 322 nm (Fig. 7) is noteworthy and the spectral position is similar to that seen with distamycin binding to an AAGTT-containing decameric duplex[26] as well as those of polyamide–DNA interactions (27). In the CD spectrum induced by

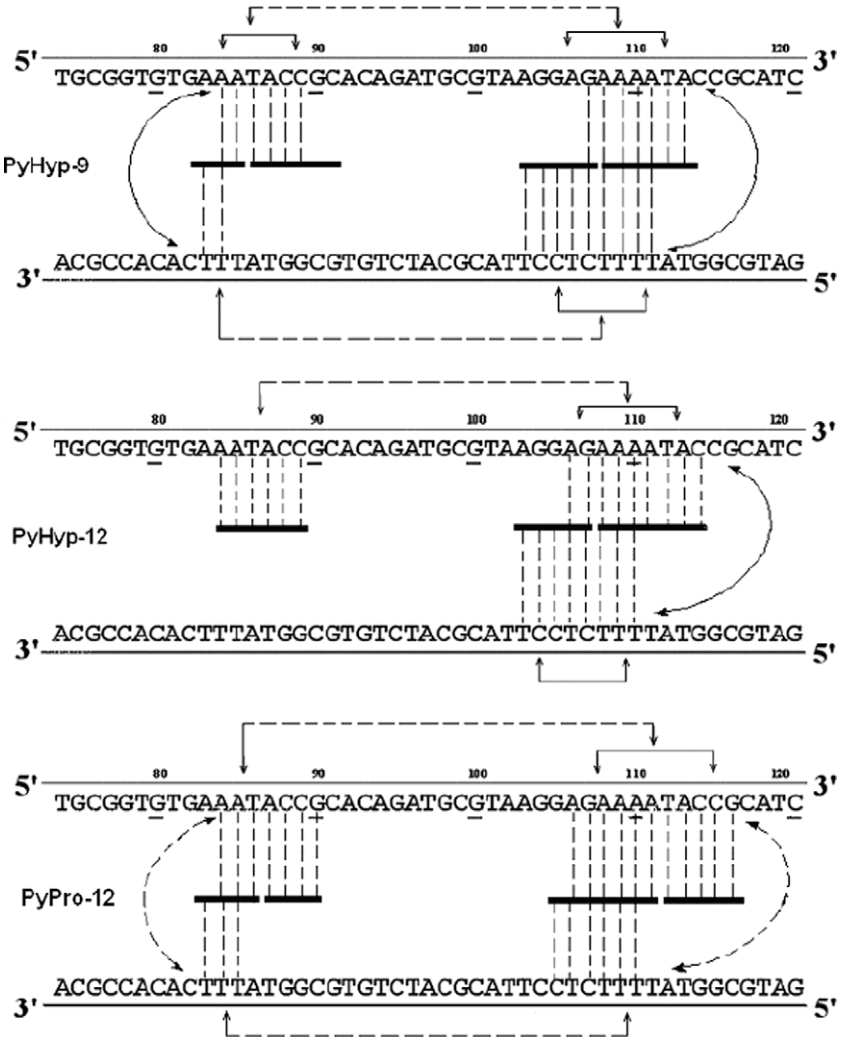

Figure 5. Proposed allosteric models for cooperative binding of peptides PyHyp-9, PyHyp-12 and PyPro-12 to 158-mer and 135-mer pBR322 fragments based on quantitative footprinting studies. The portion of the ligand binding to each DNA site/sub-site is represented by a thick horizontal line. Monodentate interactions and interstrand bidentate interactions are represented by vertical broken lines. The arrow lines represent communication of allosteric interaction between DNA binding sites. Arrow lines between the complementary strands represent possible influence of interstrand bidentate interactions mediated via DNA conformational changes. Broken arrow lines between neighboring binding loci in the top two panels are intended to represent negative cooperative communications.

DNA binding of a related peptide HR-12 (His-Pro-Arg-Lys)$_3$-NH_2, the positive CD band around 322 nm is absent (spectrum not shown). It has been demonstrated that molecules that bind to the minor groove typically elicit the appearance of a positive CD band.[27] Thus we reason that positive CD enhancement bands like those we detect around 322 nm are probably induced only by minor groove binding of ligands containing 4-amino-1-methylpyrrole-2-carboxylic acid (Py) residues. Compared to peptide PyHyp-12 with its four Py residues, peptide PyHyp-9 has only three, resulting in fewer H-bond interactions in the minor groove. Accordingly the observed change in ellipticity induced by PyHyp-9 is less than that of PyHyp-12 around 322 nm. Thus the CD spectral characterization of the binding of these peptides is consistent with the footprinting results and supports the allosteric model (Fig. 5) in which the recognition process involves cooperative binding of two peptide molecules to the d(AAAA)–d(TTTT)- or d(AAA)–d(TTT)-containing loci at appropriate [peptide]/[duplex] ratios. This accords with the finding that peptide molecules are hydrogen bonded to bases of complementary strands at these sites via interstrand bidentate interactions,[15,22] and is fully consistent with the interpretation that such interactions underlie the induction of local conformational changes in DNA as revealed by the CD experiments.

3. Conclusion

Quantitative DNase I footprinting studies have shown that network-based allostery featuring positive cooperativity appears to exist in the binding of some small peptides to adjacent sites or opposite complementary sites in DNA. However, this study also shows that allosteric communication between neighboring binding loci (separated from each other by 12–14 base pairs) can be negatively cooperative (Fig. 5, upper and middle panels). A special feature of the binding of peptides PyHyp-9 and PyPro-12 to duplex DNA molecules possessing multiple sites is the formation of a circuit type of allosteric effects within a network-based system. Unlike peptides PyHyp-9 and PyPro-12, for peptide PyHyp-12 the networks are referred to as an incomplete-circuit type. On the other hand, since peptides $(HPRK)_3NH_2$ [HR-12], and $(SPRK)_3NH_2$ [SP-12] bind to DNA fragments with GC-rich motifs lacking interstrand bidentate interactions, they form a non-circuit type of allosteric communication.[17] Thus, the present study and the previous one[17] enable us to hypothesize three different types of network-based allosteric communication in peptide–DNA molecular recognition.

The distinct positive CD bands induced by PyHyp-9 and PyHyp-12 around 288–323 nm indicate that significant local conforma-

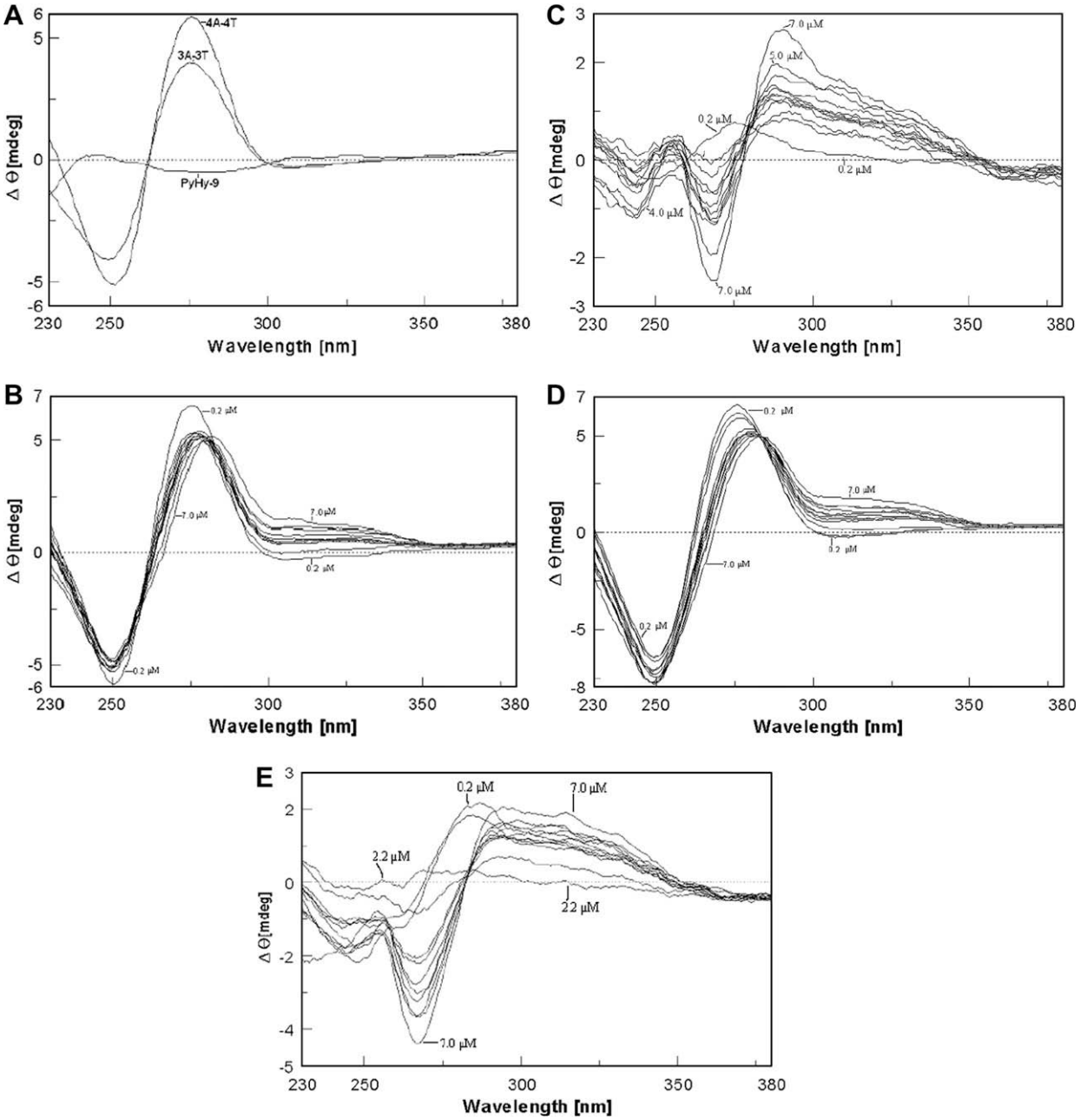

Figure 6. Panel A: CD spectra of DNA duplexes 4A–4T, 3A–3T alone and peptide PyHyp-9 alone. Panel B: titration of duplex 4A–4T versus PyHyp-9 at peptide concentrations of 0.2, 1.0. 2.2, 2.4, 2.6, 2.8, 3.0, 3.2, 3.4, 4.0, 5.0, 7.0 μM. Panel C: corresponding CD difference spectra with the contribution of duplex 4A–4T and peptide subtracted. Panel D: titration of duplex 3A–3T versus PyHyp-9 over the same peptide concentration range. Panel E: corresponding CD difference spectra with the contributions of duplex 3A–3T and peptide subtracted.

tional changes are induced in the minor groove of the helix, resulting in positive cooperative binding of peptide molecules. Enhancement of the CD bands is correlated with peptide–DNA binding stoichiometry, suggesting a three-step stoichiometric binding process proceeding from 1:1 through 2:1 to non-specific *n*:1. This study therefore helps to provide insights into the network-based nature of allostery as it affects complex DNA–small molecule interactions.

4. Experimental

Protected amino acid derivatives were purchased from Bachem California (Torrance, CA) and AnaSpec, Inc. (San Jose, CA) or synthesized in our own laboratory according to published procedures. All other analytical reagents were purchased from Acros, Tedia or Sigma. The radiolabelled nucleoside triphosphate [γ-^{32}P]ATP was obtained from NEN Life Science Products at a specific activity of 6000 Ci/mmol. *Taq* polymerase, T4 polynucleotide kinase, and DNase I were purchased from Promega. DNA undecamers were purchased from Mdbio Inc., Taipei, Taiwan. Equal equivalents of complementary strands of DNA oligomers in 5 mM sodium cacodylate buffer, pH 6.5 were annealed by heating to 94 °C for 5 min followed by slow cooling to room temperature. Other chemicals were analytical grade reagents, and all solutions were prepared using deionized, Millipore filtered water. Melting points were determined on a Mel-Temp apparatus (Cambridge, Mass) and are uncorrected. Optical rotations were determined on a Rudolph Autopol II instrument. Semi-preparative and analytical HPLC (Vy-

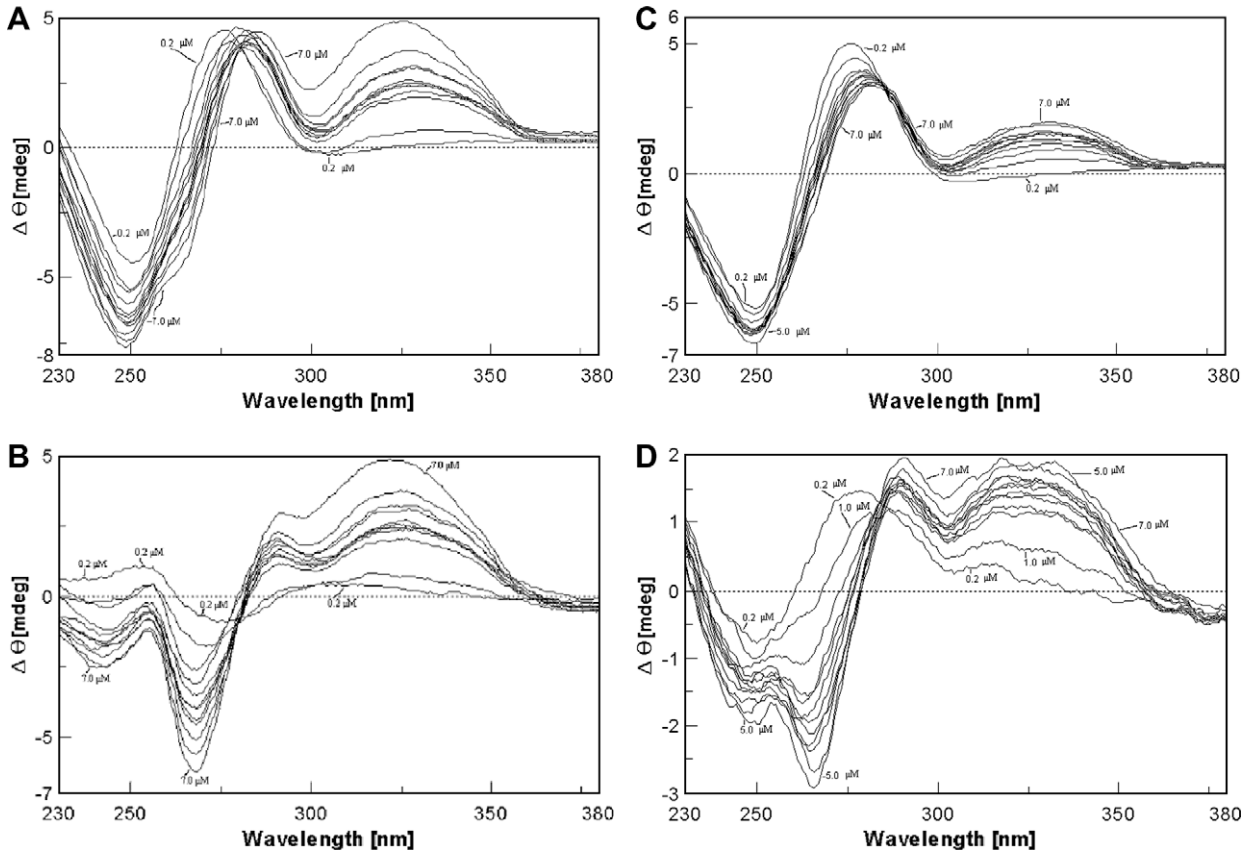

Figure 7. Panel A: titration of duplex 4A–4T versus PyHyp-12 at the same concentrations as in Figure 6B. Panel B: corresponding difference spectra with the contributions of duplex 4A–4T and peptide subtracted. Panel C: titration of duplex 3A–3T versus PyHyp-12 over the same peptide concentration range. Panel D: difference spectra with the contributions of duplex 3A–3T and peptide subtracted.

dac reversed-phase columns, TP201; column 1, 1 × 25 cm; column 2, 0.4 × 25 cm) were performed using a Hitachi L-7100 pump equipped with a gradient elution device and a Soma S-3702 variable wavelength UV detector which is connected to a PC computer installed with Hitachi HPLC analytical software. Mass spectra were determined with a Finnigan/Thermo Quest MAT 95XL instrument operating in the electrospray ionization (ESI) mode in National Chung-Hsing University.

4.1. Solid-phase peptide synthesis

4.1.1. His-Hyp-Arg-Lys-(Py)$_4$-His-Hyp-Arg-Lys-NH$_2$ (PyHyp-12)

This peptide was synthesized using solid phase methodology by manual operation of a Protein Technology PS3 peptide synthesizer. The first Fmoc-protected amino acid was coupled to the Nova Rink amide AM resin using PyBOP/NMM in DMF. All of the N_α-Fmoc-protected amino acids (in 4 equiv ratio excess to the resin) were coupled in a stepwise fashion using PyBOP/NMM in DMF after deprotection of the N_α-Fmoc group by piperidine. The side chains of Arg, Lys, Tyr and His were protected by the Pmc, Boc and Trt groups, respectively. After coupling the last *N*-terminal Fmoc-amino acid residue, the resin was treated with the cleavage reagent (0.75 g phenol, 10 mL TFA, 0.5 mL thioanisole, 0.25 mL EDT) for 1.5 h, and then lyophilized. The resin was washed first with dry ether (2 × 30 mL), filtered, and then with 5% acetic acid (200 mL). The combined filtrate was lyophilized and the product purified by semi-preparative reversed-phase HPLC (column 1) using gradient elution. Eluent A: 5% MeCN, 95% H_2O, 0.1% TFA; eluent B, 95% MeCN, 5% H_2O, 0.1% TFA. A linear gradient was achieved by increasing the MeCN content from eluent A to eluent B in 30 min. R_t (column 2), 11.59 min. Mp 154–157 °C, $[\alpha]_D^{24}$ −51.54 (*c* 0.0388, MeOH/H_2O, 1:1); ESIMS requires: 1574.75, found: 1576.0.

4.1.2. His-Hyp-Arg-Lys-(Py)$_3$-His-Hyp-Lys-Arg-NH$_2$ (PyHyp-9)

This peptide was synthesized by a procedure similar to that employed for peptide PyHyp-12. R_t (column 2), 12.43 min. Mp 150–153 °C, $[\alpha]_D^{27}$ −12.67 (*c* 0.071, H_2O); ESIMS requires: 1202.37, found: 1202.0.

4.2. Polymerase chain reaction (PCR) and end-labeling of PCR products

The pBR322 fragments: 158-mer DNA duplex (upper strand 5′-^{32}P-labeled) and 135-mer DNA duplex (lower strand 5′-^{32}P-labeled) were prepared by PCR amplification in a thermal cycler (ABI model 9700) as reported previously.[15] The sequence of the 81-mer DNA duplexes (S-81, 5′-^{32}P-labeled upper and lower strands) is shown below; these were also prepared by PCR amplification. The concentrations of DNA used as determined by UV spectroscopy are around 10^{-7} M.

```
1          10         20         30         40         50
5'-ACGTAGCGATAGCGGACTGATACTCATACTCATATCTATGGAGAAAATAC
3'-TGCATCGCTATCGCCTGACTATGAGTATGAGTATAGATACCTCTTTTATG

                   60         70         80
CGATGTCAATGTCATCAGGCGCTCTTCCGCT-3'
GCTACAGTTACAGTAGTCCGCGAGAAGGCGA-5'
```

4.3. DNase I footprinting

Reactions were conducted in a total volume of 10 μL. Briefly, radiolabelled DNA (2 μL) was mixed with varying concentrations of peptide (2 μL) dissolved in 5 mM sodium cacodylate buffer, pH 6.5) and equilibrated at room temperature for 60 min. DNase I (2 μL) was added and the reaction allowed to proceed at 37 °C for 10 min. The DNase I solution (in 20 mM NaCl, 2 mM $MgCl_2$, 2 mM $CaCl_2$) was adjusted to yield a final concentration of 0.009 unit/mL so as to limit the digestion to less than 30% of the starting material in order to minimize the incidence of multiple cleavages in any strand. The digestion was stopped by adding a solution (4 μL) containing 80% formamide, 10 mM EDTA, 0.1% bromophenol blue, and 0.1% xylene cyanol. The various samples were heated at 90 °C for 4 min and chilled on ice for 4 min and loaded on to the gel in a total volume of 10 μL/well. After electrophoresis (about 1.45 h at 70 W, 1800 V in TBE buffer, BRL sequencer model S2), gels were soaked in 10% acetic acid/10% methanol for 15 min, transferred to Whatman 3MM paper, dried under vacuum at 80 °C for 45 min, and placed against Kodak BioMax MR scientific imaging films with intensifying screens for about five days. The electrophoretic band areas were analyzed by a PC computer installed with Viber Lourmat BIO-ID software (Marne La Valle, Cedex 1, France). The apparent DNA binding site saturation is determined by the following equation:[11]

$$Y' = 1 - (I_{tot}/I_{ref})/(I^{o}_{tot}/I^{o}_{ref})$$

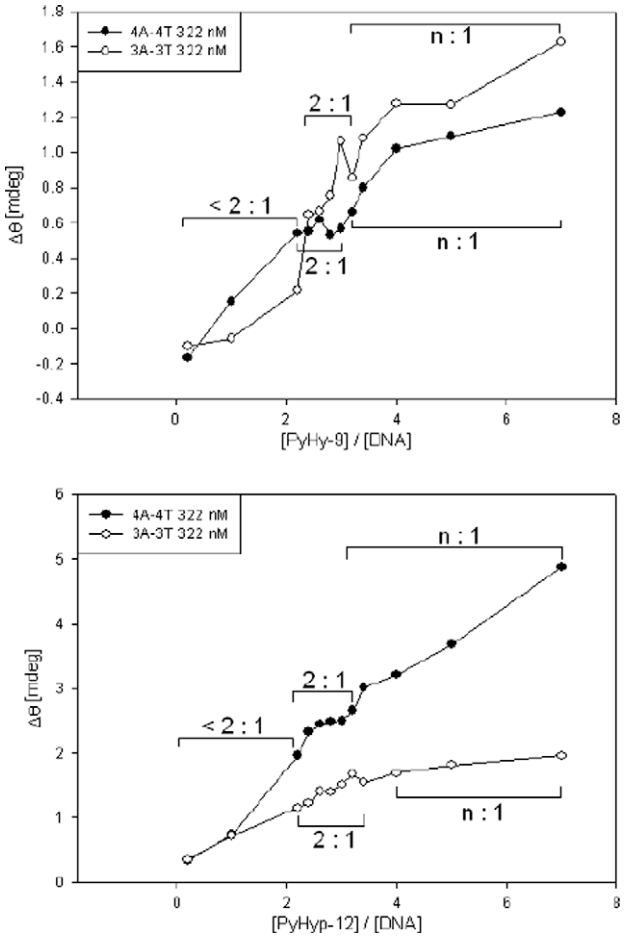

Figure 8. CD intensity at 322 nm as a function of [PyHyp-9]/[duplex] (upper panel) and [PyHyp-12]/[duplex] (lower panel). The proposed stoichiometric binding ratios are as indicated, with binding below 2:1 (<2:1) considered to be predominantly 1:1.

where Y' is the fractional saturation, I_{ref} and I^{o}_{ref} are integrated band volumes of 5 bases of a running lane (non-binding site, with peptide) and control lane (without peptide), respectively. I_{tot} and I^{o}_{tot} are integrated band volumes of the binding site locus and corresponding control lane locus, respectively.

The value of Y is optimized by the following equation:

$$Y = (Y' - Y'_{min})/(Y'_{max} - Y'_{min})$$

where Y'_{max} and Y'_{min} are the maximum and minimum site saturation Y' values, respectively.

The Hill coefficients were determined by the Hill equation:

$$\text{Log}\ [Y/1-Y] = \log K_a + n_H \log[L]$$

where $[L]$ is the peptide concentration, and n_H the Hill coefficient. At least six data points within or near the linear portion of binding isotherm (Y vs Log $[L]$) were carefully chosen for the Hill plot (Log $Y/(1-Y)$ vs Log $[L]$) using a linear least-squares fitting procedure by Sigma Plot software (version 8.0). The Hill coefficient was determined from the slope of the corresponding Hill plot. The apparent binding constant K_a is determined empirically as the peptide concentration at 50% fractional saturation from the binding isotherm.

4.4. Circular dichroism (CD) studies

CD spectra were measured at 37 °C with a Jasco J-815 instrument in the Institute of Chemistry, Academia Sinica. The duplex DNA was adjusted to 1.0 μM in 5 mM sodium cacodylate buffer (pH 6.5) and peptides, dissolved in the same buffer, were added to maintain final concentrations of 0.2, 1.0, 2.2, 2.4, 2.6, 2.8, 3.0, 3.2, 3.4, 4.0, 5.0 and 7.0 μM. CD spectra were recorded after 60 min incubation at 37 °C.

Acknowledgments

We thank Miss L. M. Hsu, National Chung-Hsing University for ESI mass analyses. This work was supported by Grant NSC93-2113-M029-003 from the National Science Council, ROC and Grant TCVGH-T-947807 to L.S.

Supplementary data

Supplementary data associated with this article can be found, in the online version, at doi:10.1016/j.bmc.2009.10.048.

References and notes

1. Fox, K. R.; Waring, M. J. *Methods Enzymol.* **2001**, *340*, 412.
2. Moravek, Z.; Neidle, S.; Schneider, B. *Nucleic Acids Res.* **2002**, *30*, 1182.
3. Bailly, C.; Chaires, J. B. *Bioconjugate Chem.* **1998**, *9*, 513. and references cited therein.
4. Waring, M. J. Echinomycin, Triostin and Related Antibiotics. In *Antibiotics*; Hahn, F. E., Ed.; Springer: Berlin, 1979; Vol. 5, pp 173–194.
5. Chaires, J. B.; Fox, K. R.; Herrera, J. E.; Britt, M.; Waring, M. J. *Biochemistry* **1987**, *26*, 8227.
6. Hudson, J. S.; Brooks, S. C.; Graves, D. E. *Biochemistry* **2009**, *48*, 4440.
7. Bailly, C.; Suh, D.; Waring, M. J.; Chaires, J. B. *Biochemistry* **1998**, *37*, 1033.
8. Chen, Y. H.; Lown, J. W. *J. Am. Chem. Soc.* **1994**, *116*, 6995.
9. Walker, W. L.; Landaw, E. M.; Dickerson, R. E.; Goodsell, D. S. *Proc. Natl. Acad. Sci. U.S.A.* **1997**, *94*, 5634.
10. Blasko, A.; Bruice, T. C. *Proc. Natl. Acad. Sci. U.S.A.* **1993**, *90*, 10018.
11. Mrksich, M.; Parks, M. E.; Dervan, P. B. *J. Am. Chem. Soc.* **1994**, *116*, 7983.
12. Fechter, E. J.; Dervan, P. B. *J. Am. Chem. Soc.* **2003**, *125*, 8476. and references cited therein.
13. Weyermann, P.; Dervan, P. B. *J. Am. Chem. Soc.* **2002**, *124*, 6872.
14. Yang, C. H.; Chou, P. J.; Luo, Z. L.; Chang, J. C.; Cheng, C. C.; Martin, C. R. H.; Waring, M. J.; Sheh, L. *Bioorg. Med. Chem.* **2003**, *11*, 3279.
15. Chang, J. C.; Yang, C. H.; Chou, P. J.; Yang, W. H.; Chou, I. C.; Lu, C. T.; Lin, P. H.; Hou, R. C. W.; Jeng, K. C. G.; Cheng, C. C.; Sheh, L. *Bioorg. Med. Chem.* **2004**, *12*, 53.
16. Yang, C. H.; Chen, W. F.; Jong, M. C.; Jong, B. J.; Chang, J. C.; Waring, M. J.; Ma, L.; Sheh, L. *J. Am. Chem. Soc.* **2004**, *126*, 8104.
17. Yang, C. H.; Jeng, K. C. G.; Yang, W. H.; Chen, Y. L.; Hung, C. C.; Lin, J. W.; Chen, S. T.; Richardson, S.; Martin, C. R. H.; Waring, M. J.; Sheh, L. *ChemBioChem.* **2006**, *7*, 1187.

18. Churchill, M. E. A.; Suzuki, M. *EMBO J.* **1989**, *8*, 4189.
19. Suzuki, M. *Nature* **1990**, *344*, 562.
20. Calvano, W. E. et al *Nature* **2005**, *437*, 1032.
21. Koshland, D. E., Jr.; Hamadani, K. *J. Biol. Chem.* **2002**, *277*, 46481. and references cited therein.
22. Luscombe, N. M.; Laskowski, R. A.; Thornton, J. M. *Nucleic Acids Res.* **2001**, *29*, 2860.
23. Ciubotaru, M.; Ptaszek, L. M.; Baker, G. A.; Baker, S. N.; Bright, F. V.; Schatz, D. G. *J. Biol. Chem.* **2003**, *278*, 5584.
24. Ouameur, A. A.; Tajmir-Riahi, H.-A. *J. Biol. Chem.* **2004**, *279*, 42041.
25. Tato, I.; Zunzunegui, S.; de la Cruz, F.; Cabezon, E. *Proc. Natl. Acad. Sci. U.S.A.* **2005**, *102*, 8156.
26. Chen, F. M.; Sha, F. *Biochemistry* **1998**, *37*, 11143.
27. Buchmueller, K. L.; Staples, A. M.; Howard, C. M.; Horick, S. M.; Uthe, P. B.; Le Minh, N.; Cox, K. K.; Nguyen, B.; Pacheco, K. A. O.; Wilson, W. D.; Moses, Lee *J. Am. Chem. Soc.* **2005**, *127*, 742.